


# Microstructure and wear analysis of CoWC alloy layers deposited by PTA process

Murat Ozabaci<sup>1</sup>, Tanju Teker<sup>2,\*</sup> , and S. Osman Yilmaz<sup>3</sup>

<sup>1</sup> Inonu University, Scientific and Technological Research Center, 44280 Malatya, Turkey

<sup>2</sup> Sivas Cumhuriyet University, Faculty of Technology, Department of Manufacturing Engineering, 58140 Sivas, Turkey

<sup>3</sup> Namık Kemal University, Faculty of Engineering, Department of Mechanical Engineering, 59860 Çorlu, Tekirdag, Turkey

Received: 28 June 2022 / Accepted: 9 January 2023

**Abstract.** CoWC composite coatings were produced on AISI 430 steel by the plasma transfer arc cladding. Three different powder mixtures containing WC (90%, 85% and 80%) and Co (10%, 15% and 20%) were used. Phase composition, microstructural characterization and coating properties were investigated by using scanning electron microscope (SEM), energy dispersive spectrometry (EDS), X-ray diffraction (XRD), elemental mapping, hardness and wear test. The wear shape morphology of coatings was determined by SEM. The increased ratio of WC in CoWC powders reduced the degradation of CoWC. The substrate hardness of 180 HV gained a coating hardness value of approximately 462 HV. An increase in the hardness of the coating alloy compared to the substrate was achieved. W<sub>2</sub>C, WC, CoC and Co<sub>6</sub>W<sub>6</sub>C phases were determined on the coating surface. The high levels of WC concentration on the coating surface increased the wear resistance.

**Keywords:** PTA / cladding / CoWC / hardness / wear

## 1 Introduction

Normal unalloyed and low-alloyed steels are not resistant to corrosive effects. Stainless steels (SS) are generally suitable for such applications. SS have qualities such as corrosion resistance, availability of types with different mechanical properties, use at low and elevated temperatures, longevity, ease of shaping, environmental friendliness and aesthetic appearance [1–3]. In the plasma transfer arc welding (PTA), a plasma with high energy density directly compressed in a short arc plasma torch is obtained. Double gas is applied in the plasma torch. The gas given from the tungsten cathode environment is called plasma gas. This gas both protects the tungsten cathode copper nozzle and ionizes ensuring the conductivity and stability of the plasma. The inert gas, argon, is usually utilized as the plasma gas. The second gas is the shielding gas. This gas is transferred between the workpiece and the torch in a way that surrounds the plasma. Duties of shielding gas: Focusing the plasma from the outside with thermal compression, increasing the energy power, also protecting the electrode and welding place from atmospheric effects. The material melted at the weld, easily solidifies as the

plasma progresses, due to surface tension behind the plasma [4–7]. Surface engineering techniques manufacture different types of composite and coating materials. Electroplating claddings, thermal sputtering, plasma and laser remelting have been reported in the literature [8–10]. Metal matrix composites (MMCs) are materials that have the superior hardness, toughness of ceramic reinforcement materials such as WC, SiC and Cr<sub>3</sub>C<sub>2</sub>. CoWC-MMC alloys are selected as hardfacing in oil, gas and agricultural industry tools due to their exceptional wear and corrosion resistance. CoWC alloys are applied for plating machine parts where corrosion and strength performance is required [11–13]. Zhou et al. reported changes in the microstructure and properties of Cr<sub>3</sub>C<sub>2</sub> alloyed with PTA on AISI 310. When the Cr<sub>3</sub>C<sub>2</sub> quantity was little, (Fe, Ni) solid solution, carbides, columnar crystal and cellular crystal appeared [14]. Deng et al. investigated the Fe-Mo alloying on AISI 1045 steel with PTA. The hardness and wear performance of the coating was greater than that of the substrate. The wear mechanism was abrasive and oxidation [15]. Jin et al. performed electro-thermal explosion directional spraying technology for WC/Co coatings. WC/Co coatings have found that it provides exceptional wear resistance [16]. Rajinikanth and Venkateswarlu reported sliding wear of mild steel sample with and without WC coating. WC coated samples exhibited excellent wear performance [17].

\* e-mail: [tanjuteker@cumhuriyet.edu.tr](mailto:tanjuteker@cumhuriyet.edu.tr)

**Table 1.** Experimental conditions used in PTA coating.

Current intensity (A)	Shielding gas flow (l/min)	Plasma gas flow (l/min)	Welding speed (m/min)
130	20	0.8	0.01

Yang et al. investigated carbide influence of grain size on the wear strength of WC-Co coatings [18]. Mutairi et al. studied coating microstructures with reactions of WC-12Co powder having micro and nano-sized. [19].

The purpose of this investigation is to determine the microstructure, hardness and wear features of the coatings produced from CoWC powder mixture on AISI 430 steel by the PTA method.

## 2 Materials and methods

AISI 430 steel (Fe: Bal., C: 0.047, Cr: 16.04, Ni: 0.21; Si: 0.42; Mn: 0.60, wt.%) specimens of  $10 \times 10 \times 10 \text{ mm}^3$  were selected as substrate. The weight percent of Co and WC particles was selected as follows: (S1) 90% WC and 10% Co, (S2) 85% WC and 15% Co, (S3) 80% WC and 20% Co. Tungsten carbide (WC) and cobalt (Co) powders were mixed. CoWC powders including dimensions between 45 and  $100 \mu\text{m}$  were used as a coating material. The powders were homogenized in a ball mill for 2 h and were dried at  $120^\circ\text{C}$  for 3 h. Before the PTA process, the surfaces of stainless steel samples were polished, and then cleaned with alcohol. The experimental conditions used in PTA coating are shown in Table 1. The PTA cladding was carried out by PTA-Thermal Dynamics PS 3000 system. Standard metallographic procedures were applied for preparation of the samples. The samples were flatted using 180–1200 mesh SiC sanding papers and polished in the polishing device using diamond paste of  $3 \mu\text{m}$ . AISI 430 substrates and the coating layers were electrolytically etched with a 10% oxalic acid solution at 5 V for 12 s. The phase composition of all samples was defined by Bruker D8 Advance X-ray diffraction (XRD) with Cu-K $\alpha$ , 40 kV, 40 mA,  $\lambda = 1.54050 \text{ \AA}$ . The microstructural changes occurring in the welded joints were identified by using a ZEISS LEO EVO LS10 scanning electron microscope (SEM), energy dispersive spectrometer (EDS), elemental mapping. Microhardness values were measured at QNESS Q10 brand device by applying a load of 50 g for 10 s. The wear performance of the samples was measured on a pin-on-disc wear machine (Model: UTS-Tribometer T10/20) with a load of 30 N and 1000 m according to ASTM-G65 standard. The wear morphology of the coatings was determined by SEM.

## 3 Results and discussion

### 3.1 Microstructure analysis

WC and cobalt powder mixture were alloyed on AISI 430 steel with the high density PTA coating. SEM micrographs of S1-S3 coatings are presented in Figures 1a–1c. The current density of PTA was taken as 130 A, and the thickness of the modified surface layer was measured for the

concentration of WC in cladding power. The thickness of modified surface was decreased with increase of WC concentration as approximately 10% for 5 wt.% WC addition. The melt solidified on the substrate surface with a high cooling rate, and a large temperature gradient occurred when the high-temperature molten pool came into contact with the matrix. On the other hand, the solidification rate of the alloy melt was low when the alloy melt started to solidify at the underside of the molten pool [20,21]. Columnar grains formation mechanism was strictly related to the temperature gradient/solidification rate. Therefore, many fine columnar grains appeared in the lower zone due to the higher temperature and lower degree of solidification rates [22,23]. The microstructure of CoWC coatings displayed mostly columnar grains in the matrix. The highest temperature gradient occurred between the bottom zone of molten pool and the substrate. The principles of solidification explain the relation of temperature gradient/solidification rate value with the grain morphology. According to these principles, the growing direction of the columnar grains was opposite of the heat diffusion. It was perpendicular to the substrate surface. On the other hand, the equiaxed grains were gradually replaced with columnar grains in the top region of the coating due to decrease of heat diffusion [24]. All samples indicated parabolic style bond line between the coating and the matrix which was an image of PTA coating, and this suggested that the applied PTA processing parameters were appropriate.

The high PTA power completely melted the powder particles on the surface and reduced the surface roughness. Cracks and pores were not revealed in macroscopic examinations. Since the coating did not delaminate, there was a good bond between the coating and the steel. Macroscopic evaluations of sample surfaces and sections showed that the matrix powder was completely dissolved during the settling operation and the WC were partially melted for especially sample S1 having high level of WC. The PTA force caused the formation of parabolic shaped bond lines between the coating and the substrate (Fig. 1). Due to heat density, the temperature gradient slowly declined. The heat radiated parallel to the upper zone of the coating layer. This changed the growth direction of columnar grains. Also, increasing the WC powder ratio for sample S3 to S1 made the columnar grains finer, where the WC powders form nucleation zones within the columnar grains in the matrix [25,26]. The carbides were distributed relatively evenly throughout the entire coating. It was seen that the XRD model of the samples was similar. Hence, the XRD model of S3 coating is demonstrated in Figure 2. The microstructure of the cladding layer consisted of WC,  $\text{W}_2\text{C}$ , CoC and  $\text{Co}_6\text{W}_6\text{C}$  phases dispersed in the  $\gamma$ -Co matrix. The micrograph of EDS analysis points of sample S3 and the elemental analysis of object 1–4 the

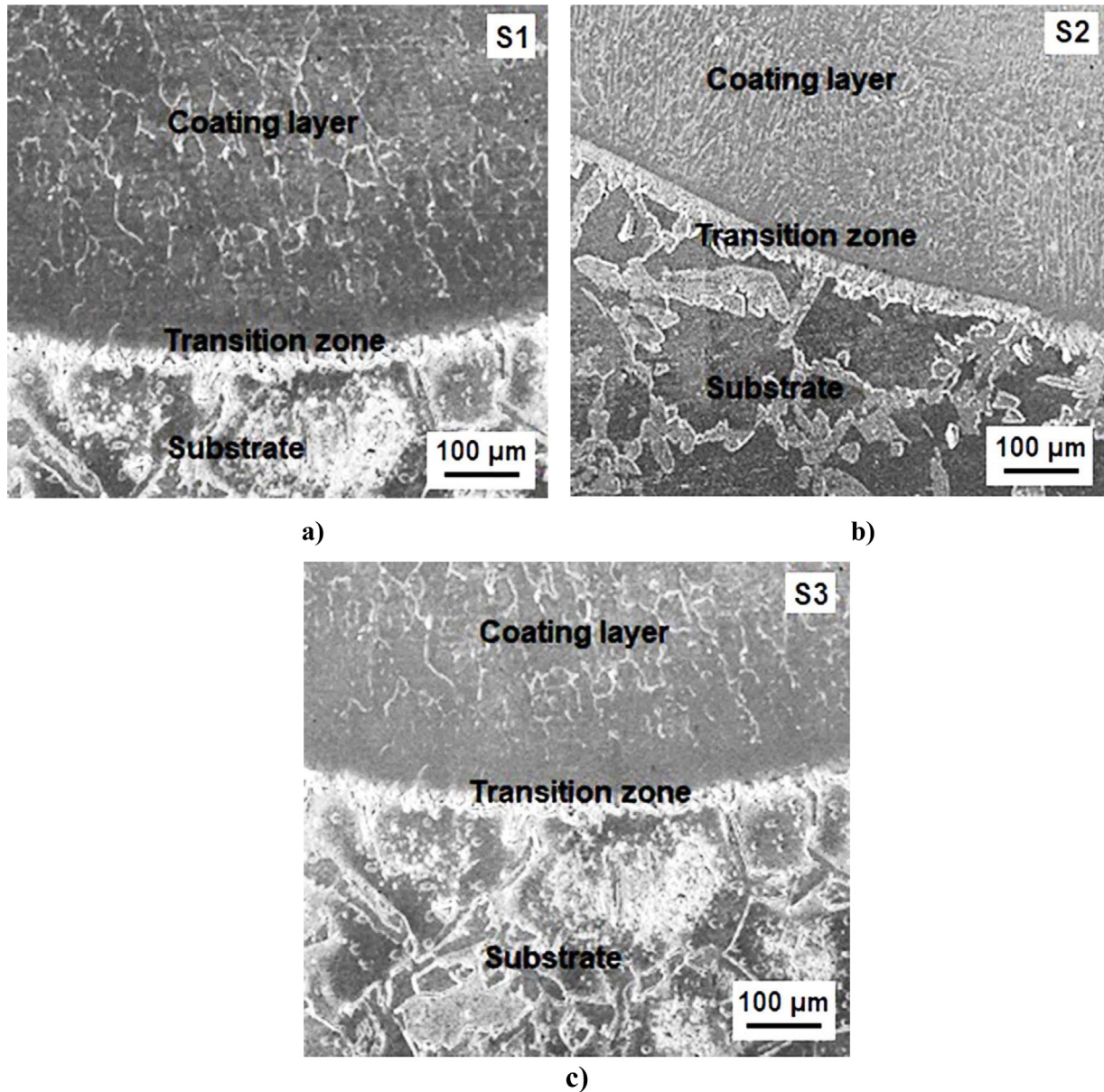


Fig. 1. SEM micrographs of (a) S1, (b) S2, (c) S3 coatings.

points are presented in Figures 3a and 3b. Object 1 composed of 45.34 wt.%Fe, 8.94 wt.%W, 29.56 wt.%Cr, 2.68 wt.%Ni, 11.87 wt.%C and 1.60 wt.%Co. Object 2 consisted of 46.15 wt.%Fe, 7.90 wt.%W, 26.30 wt.%Cr, 3.39 wt.%Ni, 14.26 wt.%C and 1.99 wt.%Co. Depending on the EDS analysis, it was thought that the spherical inclusions at grain boundaries of the modified surface were likely carbides with (Co,W)C content as labeled object 1 and 2. The tungsten rate decreased as the measuring points moved away from the carbide particles. Tungsten slowly dissolved in cobalt. Higher carbon and lesser cobalt quantity were obtained in the eutectic than in the dendritic structure (Fig. 3). It was aimed to detect the concentration of transition zone by EDS analysis of object 3–4 (Fig. 3). Object 3 included 71.37 wt.%Fe, 15.56 wt.%Cr, 2.50 wt.%

W, 3.95 wt.%Ni, 3.22 wt.%Co and 3.40 wt.%C. Object 4 consisted of 71.39 wt.%Fe, 15.03 wt.%Cr, 1.32 wt.%W, 10.51 wt.%C, 0.71 wt.%Co, 0.41 wt.%Ni and 0.64 wt.%Si. The spherical inclusions were likely carbides with (Co,W)C content. The W rate decreased as the measuring points moved away from the carbide particles.

Elemental mapping analysis of sample S3 is displayed in Figure 4. A transition zone was formed between the modified surface layer and the steel substrate. Tungsten (W), cobalt (Co), carbon (C) and iron (Fe) were the elements detected by EDS examination. A strong connection between the WC and the cobalt matrix was achieved in the coating. The carbide zone was predominantly composed of elements W and C. The substrate zone consisted of the main element Fe. The main elements of the carbide and

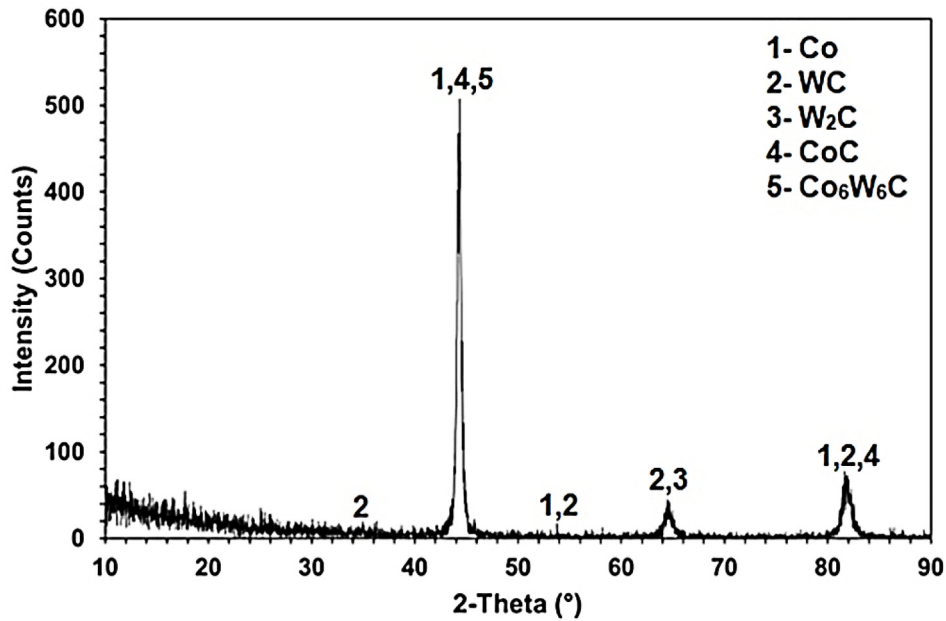


Fig. 2. XRD analysis of S3 coating.

binder compound formed the W and Co matrix. Co and WC elements migrated to the substrate material by diffusion. C, Fe from the substrate diffused into the alloy of the coating. The investigation of the cross-sectional mapping showed that the distribution of WC was not homogeneous in modified surface. The concentration of WC increased from surface to the transition zone due to the density of WC carbide (Fig. 4).

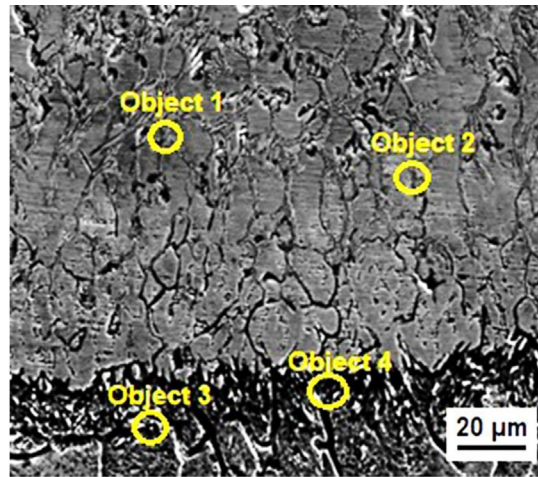
### 3.2 Hardness

Microhardness curves of CoWC powder coatings are presented in Figure 5. The hardness of the CoWC coating was considerably higher than that of AISI430 steel (180 HV) due to the WC addition and the fine grained structure formed. The melting point of the carbides was dissimilar. This difference was related to the rate and type of carbide in the matrix. The thermal conductivity of Co powder was 14.82 W/(mK) and tungsten carbide was 84.02 W/(mK) [27]. This allowed greater heat transfer to the substrate and better mixing with additives. The coating was separated dendrites that occurred at various cooling rates across the cross section of the coating. WC primary carbides enriched the matrix with carbon and tungsten by diffusion. High microhardness was accomplished by reducing the carbide particles in the matrix to a relatively small shape by the force of the plasma. In the lower part of the coating, the substrate and coating products alloyed with each other. The hardness of the fabricated coating decreased. Under the influence of the heat provided by the PTA power, WC, Co and primary carbides melted in the surface layer. W and C found in the WC diversified the element ratio of the

matrix. Throughout solidification, the matrix crystallized and spherical precipitates containing W and C were identified. The hardness, increased as the  $W_2C$  level rised. Hardness was greater when the  $Co_6W_6C$  replaced Co which was a the matrix.

### 3.3 Wear

The wear rates of the samples are shown in Figure 6. The high levels of WC powders concentration on the coating surface increased the wear resistance. These results were consistent with widely varying coating hardness. The distribution and rate of WC particles were very important in WC-Co composite coating. Due to the mixing effect in the melt pool, WC particles settled to the underside of the coating. The amount of wear increased with increment of sliding distance. Cracking and chipping of WC particles were observed in the coatings. The metallic cobalt matrix in the coating was soft and ductile. It formed a thin coating on smooth interfaces that acted as a lubricant, reducing wear rates [28,29]. Carbide fragmentation and shrinkage rates were high. Surface damage caused by deformation of Co was less at high shear speeds. As a result, the WC caused the particles to break, making wear more difficult. Hard phases such as WC and  $W_2C$  in the coating were brittle. Normal and tangential stresses took place once the wear occurred. During wear, the cobalt matrix firstly deformed and then it formed a thin lubricant layer that increased wear resistance. As the slip distance increased, matrix removal, microcracks, and carbide particle separation occurred. It caused increment of wear resistance at high speeds, as the frictional heat formed a protective oxide film.



a)

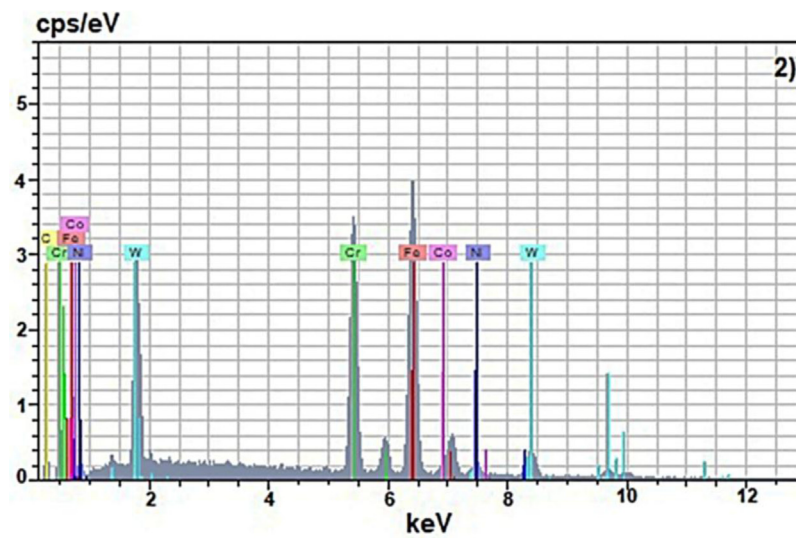
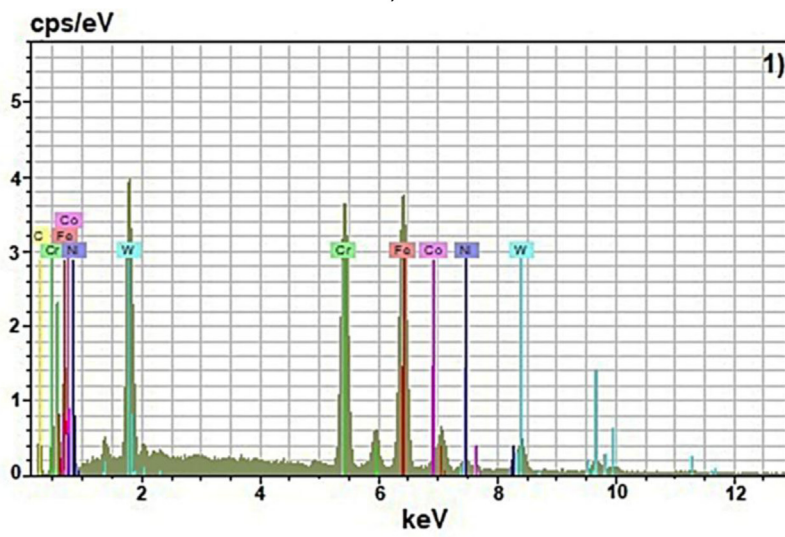


Fig. 3. (a) The micrograph of EDS analysis points of sample S3. (b) Elemental analysis of object 1-4 the points.

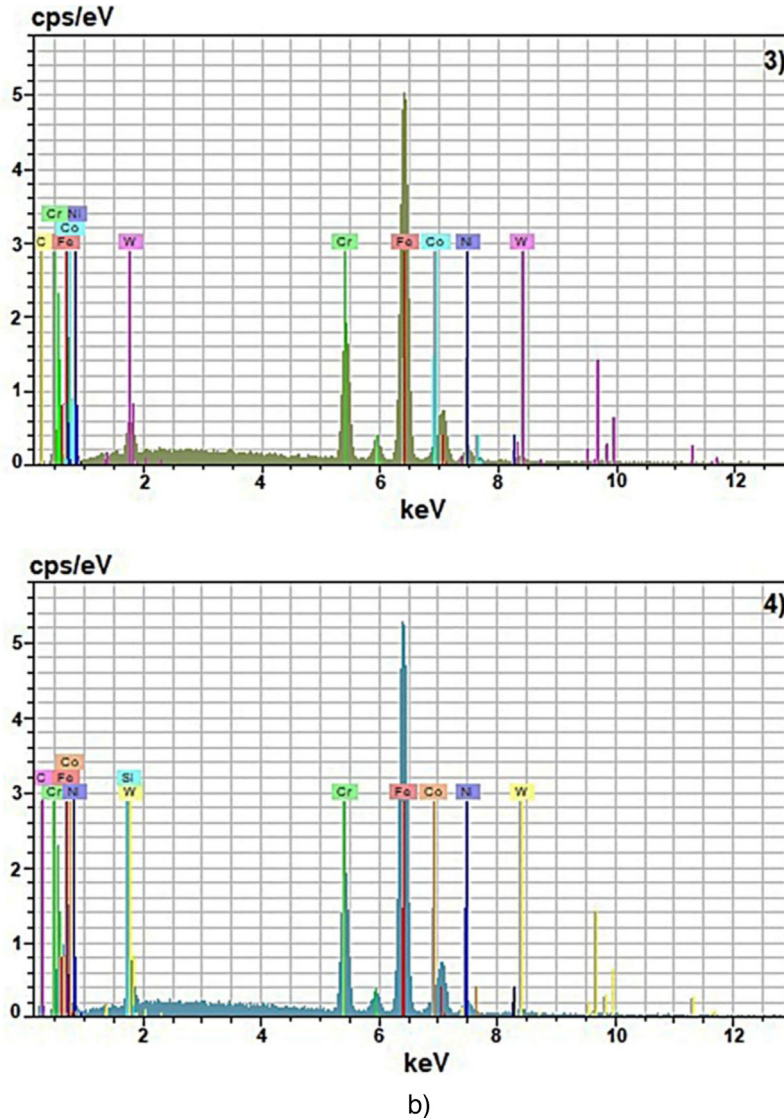


Fig. 3. Continued

The wear shape morphology of S3 coating is demonstrated in Figure 7. The wear was greater as the contact pressure of the load increased. Surface roughness consisted of WC powders and cobalt binder. During wear, a high local stress occurred at the contact points [30,31]. Removing the roughness led to the formation of chips. The soft Co matrix between the WC particles was deformed and removed from the coating. Micro-cracking and/or shrinkage occurred in WC particles and wear residues were seen.

#### 4 Conclusion

Microstructural characterization and wear properties of different CoWC powder concentration coatings produced with PTA on AISI 430 steel was investigated.

The CoWC powder mixture was successfully coated on AISI 430 steel by PTA technique.

The microstructure of the coating layer consisted of WC,  $W_2C$ , CoC and  $Co_6W_6C$  phases dispersed in the  $\gamma$ -Co matrix.

A seamless bond was obtained between WC and  $\gamma$ -Co matrix in the coating surface.

The increased WC ratio in the powder mixture increased the hardness of the coating layer.

The increase of the tungsten carbide ratio changed the matrix limits where spheriform or irregularly shaped precipitates were concentrated.

The cobalt matrix, which formed a thin layer of lubricant caused increment of wear resistance.

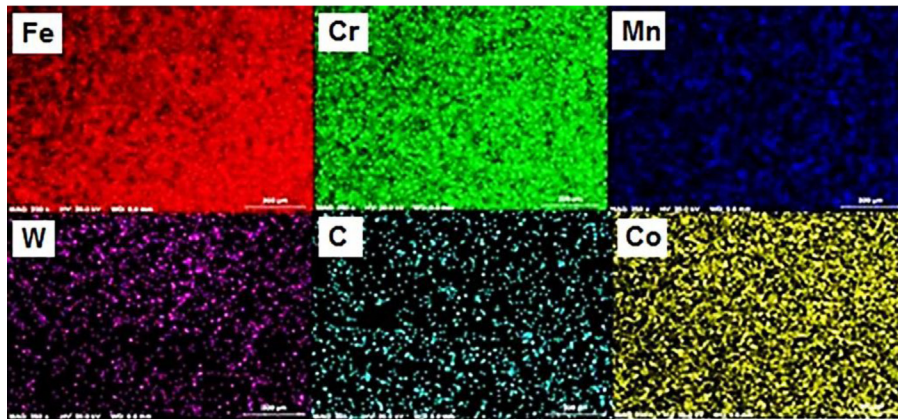
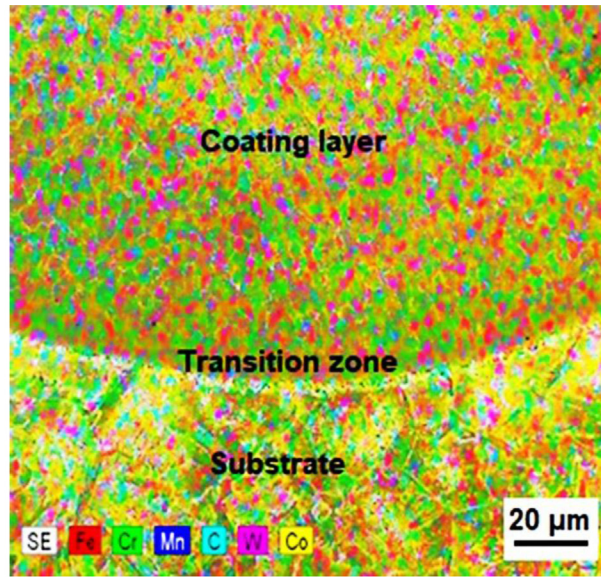


Fig. 4. Elemental mapping analysis of S3 sample.

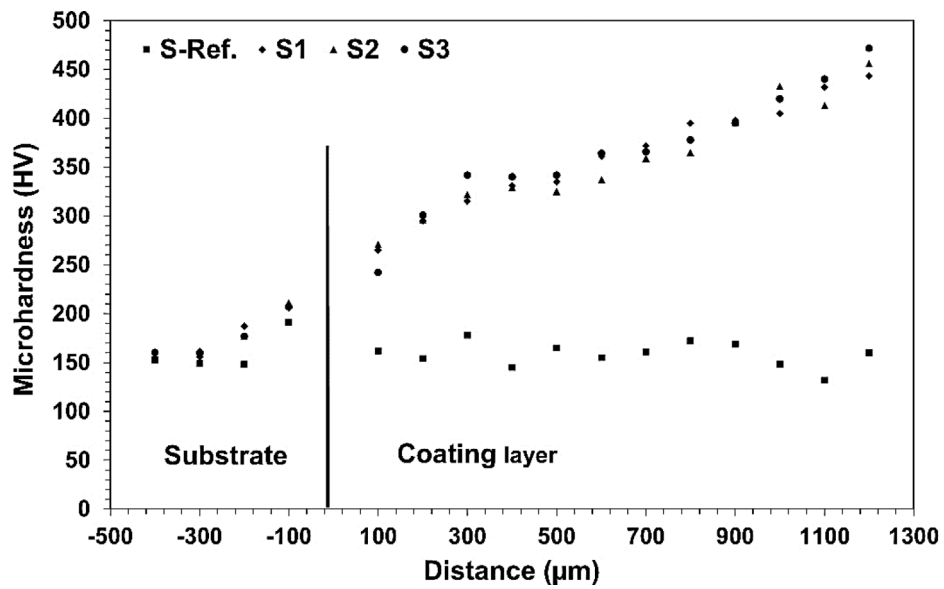


Fig. 5. Microhardness curves of coated surface and substrate for sample S-Ref, S1, S2 and S3.

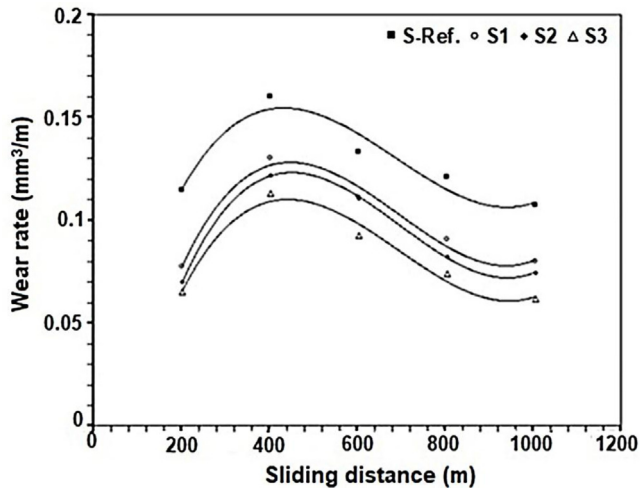


Fig. 6. Wear rates of test samples.

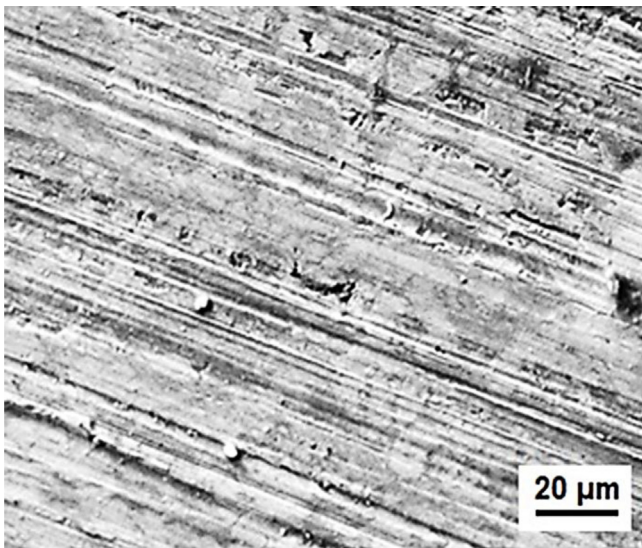


Fig. 7. Wear shape morphology of S3 coating.

## Author contributions

All the authors have accepted responsibility for the entire content of this submitted manuscript and approved submission.

## Funding

None declared.

## Disclosure statement

No potential conflict of interest was reported by the authors.

*Acknowledgements.* The authors are grateful to Inan Machine Industry and Trade Incorporate Company for their assistance in conducting the experiments.

## References

1. S. Zhou, X. Dai, H. Zheng, Microstructure and wear resistance of Fe-based WC coating by multi-track overlapping laser induction hybrid rapid cladding, *Opt. Laser. Technol.* **44**, 190 (2012)
2. M. Zhong, W. Liu, K. Yao et al., Microstructural evolution in high power laser cladding of Stellite6 WC layers, *Surf. Coat. Technol.* **2–3**, 128 (2002)
3. R. Jendrzewski, C. Navas, A. Conde et al., Properties of laser-cladded stellite coatings prepared on preheated chromium steel, *Mater. Des.* **29**, 187 (2008)
4. W.C. Lin, C. Chen, Characteristics of thin surface layers of cobalt-based alloys deposited by laser cladding, *Surf. Coat. Technol.* **14–15**, 4557 (2006)
5. A. Zielinski, H. Smolenska, W. Serbinski et al., Characterization of the Co-base layers obtained by laser cladding technique, *J. Mater. Process. Technol.* **164–165**, 958 (2005)
6. E. Díaz, J.M. Amado, J. Montero et al., Comparative study of Co-based alloys in repairing low Cr-Mo steel components by laser cladding, *Phys. Proc.* **39**, 368 (2012)
7. D. Bartkowski, A. Młynarczyk, A. Piasecki et al., Microstructure, microhardness and corrosion resistance of Stellite-6 coatings reinforced with WC particles using laser cladding, *Opt. Laser. Technol.* **68**, 191 (2015)
8. D. Bartkowski, A. Bartkowska, Wear resistance in the soil of Stellite-6/WC coatings produced using laser cladding method, *Int. J. Refract. Met. Hard Mater.* **64**, 20 (2017)
9. Q. Li, T.C. Lei, W.Z. Chen, Microstructural characterization of WCp reinforced Ni-Cr-B-Si-C composite coatings, *Surf. Coat. Technol.* **114**, 285 (1999)
10. S.O. Yılmaz, T. Teker, CoNiCrMo, FeCrNi, NiCr and FeNiAlMo modified iron based alloy coating deposited by plasma transferred arc process, *J. Optoelectron. Adv. Mater.* **15**, 1010 (2013)
11. M. Zhong, W. Liu, K. Yao et al., Microstructural evolution in high power laser cladding of Stellite 6+WC layers, *Surf. Coat. Technol.* **157**, 128 (2002)
12. J. Nurminen, J. Näkki, P. Vuoristo, Microstructure and properties of hard and wear resistant MMC coatings deposited by laser cladding, *Int. J. Refract. Met. Hard Mater.* **27**, 472 (2009)
13. T. Teker, S. Karatas, S.O. Yılmaz, The coating of FeB, FeTi, FeW powders on AISI 430 stainless steel by PTA, *J. Optoelectron. Adv. Mater.* **15**, 284 (2013)
14. Y. Zhou, Q. Wang, G. Zhang, Effect of Cr<sub>3</sub>C<sub>2</sub> content on microstructure and properties of 310 stainless steel coating by PTA welding, *Surf. Eng.* **37**, 464 (2021)
15. X. Deng, G. Zhang, T. Wang et al., Investigations on microstructure and wear resistance of Fe-Mo alloy coating fabricated by plasma transferred arc cladding, *Surf. Coat. Technol.* **350**, 480 (2018)
16. G. Jin, B. Xu, H. Wang et al., Characterization of WC/Co coatings on metal substrates, *Mater. Lett.* **61**, 24543 (2007)
17. V. Rajinikanth, K. Venkateswarlu, An investigation of sliding wear behaviour of WC-Co coating, *Tribol. Int.* **44**, 1711 (2011)



18. Q. Yang, T. Senda, A. Ohmori, Effect of carbide grain size on microstructure and sliding wear behavior of HVOF-sprayed WC-12% Co coatings, *Wear* **254**, 23 (2003)
19. S. Al-Mutairi, M.S.J. Hashmi, B.S. Yilbas et al., Microstructural characterization of HVOF/plasma thermal spray of micro/nanoWC-12%Co powders, *Surf. Coat. Technol.* **264**, 175 (2015)
20. R. Ahmed, O. Ali, N.H. Faisal et al., Sliding wear investigation of suspension sprayed WC-Co nanocomposite coatings, *Wear* **322**, 133 (2015)
21. G. Ghosh, A. Sidpara, P.P. Bandyopadhyay, High efficiency chemical assisted nano finishing of HVOF sprayed WC-Co coating, *Surf. Coat. Technol.* **334**, 204 (2018)
22. J. Yang, M. Odén, M.P.J. Jõesaar et al., Mechanical strength of ground WC-Co cemented carbides after coating deposition, *Mater. Sci. Eng. A* **689**, 72 (2017)
23. U. Selvadurai, P. Hollingsworth, I. Baumann et al., Influence of the handling parameters on residual stresses of HVOF sprayed WC-12Co coatings, *Surf. Coat. Technol.* **268**, 30 (2015)
24. T.G. Wang, S.S. Zhao, W.G. Hua et al., Estimation of residual stress and its effects on the mechanical properties of detonation gun sprayed WC-Co coatings, *Mater. Sci. Eng. A* **527**, 454 (2010)
25. G. Wang, J. Zhang, R. Shu et al., High temperature wear resistance and thermal fatigue behavior of Stellite-6/WC coatings produced by laser cladding with Co-coated WC powder, *Int. J. Refract. Met. Hard Mater.* **81**, 63 (2019)
26. J. Song, Q. Deng, C. Chen et al., Rebuilding of metal components with laser cladding forming, *Appl. Surf. Sci.* **252**, 7934 (2006)
27. J.M. Guilemany, J.M. Miguel, S. Vizcaino et al., Role of three-body abrasion wear in the sliding wear behaviour of WC-Co coatings obtained by thermal spraying, *Surf. Coat. Technol.* **140**, 141 (2001)
28. E. Sánchez, E. Bannier, M.D. Salvador et al., Microstructure and wear behavior of conventional and nanostructured plasma-sprayed WC-Co coatings, *J. Therm. Spray Technol.* **19**, 964 (2010)
29. S. Yin, E.J. Ekoi, T.L. Lupton et al., Cold spraying of WC-Co-Ni coatings using porous WC-17Co powders: formation mechanism, *Mat. Des.* **126**, 305 (2017)
30. Q. Yang, T. Senda, A. Hirose, Sliding wear behavior of WC-12% Co coatings at elevated temperatures, *Surf. Coat. Technol.* **200**, 4208 (2006)
31. G. Ghosh, A. Sidpara, P.P. Bandyopadhyay, Understanding the role of surface roughness on the tribological performance and corrosion resistance of WC-Co coating, *Surf. Coat. Technol.* **378**, 125080 (2019)

**Cite this article as:** Murat Ozabaci, Tanju Teker, S.Osman Yılmaz, Microstructure and wear analysis of CoWC alloy layers deposited by PTA process, *Metall. Res. Technol.* **120**, 211 (2023)